

Detection and characterization of multipartite entanglement in optical lattices

R.N. Palmer,¹ C. Moura Alves,¹ and D. Jaksch¹

¹*Clarendon Laboratory, University of Oxford, Parks Road, Oxford OX1 3PU, UK.*

(Dated: August 18, 2018)

We investigate the detection and characterization of entanglement based on the quantum network introduced in [Phys. Rev. Lett. **93**, 110501 (2004)] for different experimental scenarios. We first give a detailed discussion of the ideal scheme where no errors are present and full spatial resolution is available. Then we analyze the implementation of the network in an optical lattice. We find that even without any spatial resolution entanglement can be detected and characterized in various kinds of states including cluster states and macroscopic superposition states. We also study the effects of detection errors and imperfect dynamics on the detection network. For our scheme to be practical these errors have to be on the order of one over the number of investigated lattice sites. Finally, we consider the case of limited spatial resolution and conclude that significant improvement in entanglement detection and characterization compared to having no spatial resolution is only possible if single lattice sites can be resolved.

PACS numbers: 03.75.Gg, 03.67.Mn

I. INTRODUCTION

Multipartite entanglement is an essential ingredient for complex quantum information processing (QIP) tasks, such as quantum error-correction [1], multi-party quantum communication [2] and universal quantum computation in the one-way model [3]. It has been generated between photons [4] and in a controlled way both in ion traps [5] and in experiments with Mott insulating states of neutral bosonic atoms in optical lattices [6, 7]. For photon and ion trap experiments full state tomography [4, 8] impressively proved the existence of multipartite entanglement with few particles. However, its unambiguous detection in optical lattice setups has so far not been possible. The measurements implemented in the actual experiments only provided information on the average density operator of each individual atom (representing a qubit), but not on the density operator of the composite system [6]. Full state tomography in optical lattices seems to be infeasible due to the large number of involved atoms and thus other methods are required to prove the existence of entanglement. Recently, a quantum network that can detect multipartite entanglement in bosons, and can be realized in optical lattices, was proposed [9].

This quantum network is made up of pairwise beam-splitters (BS) acting on two identical copies of a multipartite entangled state $\rho_{12\dots n}$ of n atoms, and allows the determination of the purity of $\rho_{12\dots n}$ and of all its reduced subsystems. The purities provide us with a separability criterion based on entropic inequalities [9] that, if violated, indicate that the state $\rho_{12\dots n}$ is entangled. This nonlinear entanglement test can be implemented experimentally with a number of copies of $\rho_{12\dots n}$ independent of n , rather than the exponentially large number of copies needed for a full state tomography, and is more powerful than the other common experimental methods, such as Bell inequalities [10] and entanglement witnesses [11]. In fact, the nonlinear inequalities are known to be strictly stronger than the Bell-CHSH inequalities [12]. Further-

more, if it may be assumed that the entangled state is characterized by a few parameters only it is often possible to determine them from the results obtained from the entanglement detection network.

The main aim of this paper is to analyze the operation of the entanglement detection network under realistic experimental conditions. After introducing the ideal scheme we consider the particular realization of the network in an optical lattice. We discuss three main sources of imperfections: limited or no spatial resolution, errors in the BS operations occurring with a probability q , and failure to detect an atom with probability p . In current experiments none of these errors can be suppressed completely and thus it is important to find out whether their presence still allows the unambiguous detection and characterization of multipartite entangled states. Our main results will be that (i) even without spatial resolution it is possible to unambiguously detect and characterize entanglement in multipartite states like cluster states and macroscopic superposition states, (ii) the effects of BS and detection errors can be made arbitrarily small by increasing the number of runs of the entanglement detection network, and (iii) the required number of experimental runs for achieving this is reasonably small if $kq \lesssim 1$ and $kp \lesssim 1$, where $k \leq n$ is the number of particles in the subsystem whose reduced purity is being measured. Finally we will find that (iv) single site resolution is necessary to achieve significant improvement compared to having no spatial resolution at all.

The paper is organized as follows: in Sec. II we introduce the entropic inequalities and discuss how multipartite entanglement can be detected and characterized by them. Then we describe the entanglement detection network and show how it can be realized in optical lattices and how the main sources of imperfections arise. In Sec. III we investigate the detection and characterization of multipartite entangled states if no spatial resolution is available, and in Sec. IV we analyze the effect of the dominant experimental errors. We also discuss the case

of limited spatial resolution in the measurements. Finally we summarize our results in Sec. V.

II. ENTANGLEMENT DETECTION AND CHARACTERIZATION IN OPTICAL LATTICES

In this section we first present the entropic inequalities which are used to detect multipartite entanglement. We show how they can be utilized to characterize multipartite entanglement if the entangled state is described by few parameters only. Then we introduce our entanglement detection network and discuss its implementation in optical lattices. Finally we study the main types of imperfections and resulting errors that we expect to be present in this experimental realization.

A. Entropic inequalities

Our network uses the entropic inequalities introduced in [9] for multipartite entanglement detection. These inequalities provide a set of necessary conditions for separability in multipartite states. Consider a state $\rho_{123\dots n}$ of n subsystems. If $\rho_{123\dots n}$ is separable, then

$$\rho_{123\dots n} = \sum_{\ell} C_{\ell} \rho_1^{\ell} \otimes \rho_2^{\ell} \otimes \rho_3^{\ell} \otimes \dots \otimes \rho_n^{\ell}, \quad (1)$$

where ρ_j^{ℓ} is a state of subsystem j , and $\sum_{\ell} C_{\ell} = 1$. The purity $\text{Tr} \{\rho_B^2\}$ of the reduced density operator ρ_B with $B \subseteq \{1, 2, \dots, n\}$ is less than or equal to the purity of any of its reduced density operators:

$$\text{Tr} \{\rho_A^2\} \geq \text{Tr} \{\rho_B^2\} \text{ for all } A \subseteq B. \quad (2)$$

We can use these inequalities to give a relation between the average purities of all reduced density operators of a given number k of subsystems defined by

$$\overline{\text{Tr} \{\rho_{(k)}^2\}} = \left[\binom{n}{k} \right]^{-1} \sum_{|B|=k} \text{Tr} \{\rho_B^2\}, \quad (3)$$

where B is summed over all combinations of k subsystems. For completeness we define $\overline{\text{Tr} \{\rho_{(0)}^2\}} \equiv 1$. From Eq. (2) we find that for any separable state

$$\overline{\text{Tr} \{\rho_{(k)}^2\}} \geq \overline{\text{Tr} \{\rho_{(k')}^2\}} \text{ for all } k \leq k'. \quad (4)$$

We will now consider how Eqs. (2, 4) can be used to detect entanglement and to characterize entangled states.

1. Entanglement detection

Any state ρ that violates any of the inequalities Eqs. (2, 4) is entangled. If $\rho_{123\dots n}$ is separable and pure,

$\text{Tr} \{\rho_{123\dots n}^2\} = 1$ and all the above inequalities become equalities; since a state with all $\text{Tr} \{\rho_B^2\} = 1$ is necessarily a product state, all pure entangled states violate Eqs. (2, 4). All pure entangled states can hence be detected by comparing $\overline{\text{Tr} \{\rho_{123\dots n}^2\}}$ with any other $\overline{\text{Tr} \{\rho_B^2\}}$ or $\overline{\text{Tr} \{\rho_{(k)}^2\}}$ unlike entanglement witnesses or Bell inequalities where different states often require different witnesses. From the Schmidt decomposition of any pure state into two disjoint subsystems A and B with $A \cup B = \{1, 2, \dots, n\}$ we find $\text{Tr} \{\rho_A^2\} = \text{Tr} \{\rho_B^2\}$ and hence $\overline{\text{Tr} \{\rho_{(k)}^2\}} = \overline{\text{Tr} \{\rho_{(n-k)}^2\}}$ for all pure ρ .

Mixed entangled states do not always violate Eqs. (2, 4), but since $\text{Tr} \{\rho_B^2\}$ is continuous in ρ a sufficiently small amount of noise added to a pure entangled state will leave it still violating the inequalities. In the examples studied in this paper the noise level at which the inequalities no longer detect entanglement is a large fraction of the level at which entanglement ceases to be present. The permissible range values for the purities of any state ρ is

$$2^{-k} \leq \text{Tr} \{\rho_B^2\} \leq 1 \quad \text{or} \quad 2^{-k} \leq \overline{\text{Tr} \{\rho_{(k)}^2\}} \leq 1, \quad (5)$$

where $k = |B|$. The minimum is attained by the maximally mixed state $\rho = 2^{-n} \mathbb{I}$ (with \mathbb{I} the identity operator) and the maximum by any pure product state.

Our test can often verify that a state is truly n -particle entangled and not just a collection of small entangled subsystems, because $\text{Tr} \{\rho_B^2\} < \text{Tr} \{\rho^2\}$ always indicates that B is entangled with the rest of the system and cannot be caused by entanglement within B itself. Furthermore our test is insensitive to local unitary operations, which cannot alter the entanglement structure, since they do not change the purities. It is, however, in most cases sensitive to local measurements destroying entanglement as these generally do change the purities. If the tested state ρ is of a known form and characterized by few parameters only the kind and degree of violation of Eqs. (2, 4) can be used to determine these parameters and thus characterize the state.

2. Characterization of entanglement: Macroscopic superposition states

Macroscopic superposition states $|\gamma_n\rangle$ defined by

$$|\gamma_n\rangle = \frac{|0\rangle^n + (\gamma|0\rangle + \sqrt{1-|\gamma|^2}|1\rangle)^n}{\sqrt{2 + \gamma^n + \bar{\gamma}^n}}, \quad (6)$$

with a single complex parameter γ satisfying $|\gamma| \leq 1$ arise naturally in several systems such as BECs [13] and superconductors [14]. The quantity $n(1 - |\gamma|^2)$ has been suggested as a measure of the effective size of the state, as in some respects $|\gamma_n\rangle$ is equivalent to a maximally entangled state of $n(1 - |\gamma|^2)$ particles [15]. The purities

of $|\gamma_n\rangle$ are given by

$$\text{Tr} \{ \rho_B^2 \} = \frac{2 + 2\gamma^k \bar{\gamma}^k + 2\gamma^{n-k} \bar{\gamma}^{n-k}}{(2 + \gamma^n + \bar{\gamma}^n)^2} + \frac{4\gamma^n + 4\bar{\gamma}^n + \gamma^{2n} + \bar{\gamma}^{2n}}{(2 + \gamma^n + \bar{\gamma}^n)^2}, \quad (7)$$

where $k = |B|$. These purities violate Eq. (2), showing that $|\gamma_n\rangle$ is entangled, for all $|\gamma| < 1$ and measuring the purities allows determining γ . For $\gamma = 0$ the state $|\gamma_n\rangle$ is a maximally entangled state which is pure ($\text{Tr} \{ \rho^2 \} = 1$) while all its subsets have purity $\text{Tr} \{ \rho_B^2 \} = 1/2$. Up to local unitaries it is the only state with these purities, so can be unequivocally identified by our test.

We demonstrate the effect of noise on our method by studying individual dephasing of each qubit. Such dephasing noise maps a state according to

$$\rho \rightarrow \sum_A \left(1 - \frac{d}{2}\right)^{n-|A|} \left(\frac{d}{2}\right)^{|A|} \left(\prod_{j \in A} \sigma_{z,j}\right) \rho \left(\prod_{j \in A} \sigma_{z,j}\right), \quad (8)$$

where $\sigma_{z,j}$ is a phase flip applied to qubit j , A is the set of qubits which undergo a phase flip and $0 \leq d \leq 1$ is the decoherence parameter. Applying the map Eq. (8) to $|\gamma = 0\rangle_n$ we find for the resulting density operator

$$\rho = \frac{1}{2} (|0\rangle^n \langle 0|^n + |1\rangle^n \langle 1|^n) + \frac{(1-d)^n}{2} (|0\rangle^n \langle 1|^n + |1\rangle^n \langle 0|^n), \quad (9)$$

and thus $\text{Tr} \{ \rho^2 \} = (1 + (1-d)^{2n})/2$ while $\text{Tr} \{ \rho_B^2 \} = 1/2$ for all subsets B . Therefore entanglement is detected whenever it is present. This is not generally the case as can easily be seen by looking at a Werner state $\rho = (1-d)|\gamma = 0\rangle_n \langle \gamma = 0|_n + 2^{-n}d \mathbb{I}$ for which entanglement is detected if $d < 1 - (2^{n-1} + 1)^{-1/2}$. However, e.g. in the case $n = 2$ this state is entangled iff $d < 2/3$ [16], while our test works only for $d < 1 - 1/\sqrt{3}$.

3. Characterization of entanglement: Cluster states

Cluster and graph states are multipartite entangled states which form the basic building blocks of the one-way quantum computer [3]. We consider cluster-like states $|\phi_n\rangle$ defined by

$$|\phi_n\rangle = \frac{1}{\sqrt{2^n}} \prod_{j=1}^n (|0\rangle_j e^{i\phi\sigma_{z,j+1}} + |1\rangle_j) = \frac{1}{\sqrt{2^n}} \sum_{x=0}^{2^n-1} e^{i\phi c(x)} |x\rangle, \quad (10)$$

where $c(x)$ is the number of occurrences of the sequence 01 in the n -bit binary number x . These states have already been created in optical lattices [6] and represent a cluster state for $\phi = \pi$. Current methods for detecting them essentially perform a tomographic measurement

of the average single particle density matrix, which goes from pure ($|0\rangle + |1\rangle$)($\langle 0| + \langle 1|$)/2 at $\phi = 0$ to maximally mixed $\mathbb{I}/2$ at $\phi = \pi$ and back again at $\phi = 2\pi$. This method thus yields one measurement $\text{Tr} \{ \rho_{(1)}^2 \}$ relating to entanglement and two measurements relating to local unitaries.

Our network permits the measurement of further correlations and it does not need the assumption that all atoms have the same single particle density matrix. It therefore allows a better characterization of $|\phi_n\rangle$. For any ϕ which is not an integer multiple of 2π , $|\phi_n\rangle$ is a pure state with no separable subsystems, and hence for any subset B we have $\text{Tr} \{ \rho_B^2 \} < 1 = \text{Tr} \{ \rho^2 \}$ as can be seen from Fig. 1. For creating the states $|\phi_n\rangle$ each qubit only needs to interact with their two nearest neighbors except for the two extremal atoms 1 and n which will interact with only their one neighbor. Because of this the reduced purity of a subset B is determined by the boundary between it and the rest of the system. Subsets of different sizes but with the same boundary structure have the same purity. Several examples of these purities are shown in Fig. 1 as a function of ϕ . For example, all sets of two or more adjacent atoms, located anywhere in the row that do not include either extremal atom have the same purity $(1 + \cos^2(\phi/2))^2/4$ (dash dotted curve in Fig. 1) which is independent of n . The degree of violation of Eq. (2) varies smoothly with ϕ and measuring the various different purities allows to determine ϕ (up to its sign). We will now introduce a quantum network which detects violations of Eq. (2) and later, in Sec. III, show how violations of Eq. (4) can be detected even without achieving spatial resolution of the different subsystems.

B. Multipartite Entanglement Detection Network

A family of quantum interferometric networks that directly estimates $\text{Tr} \{ \rho^s \}$, $s = 2, 3, 4, \dots$ for any ρ from s copies of ρ was introduced in [17]. These networks rely on the controlled-shift operation $C - V^{(s)}$ between the different copies, where $V^{(s)} |\phi_1\rangle |\phi_2\rangle \dots |\phi_s\rangle = |\phi_s\rangle |\phi_1\rangle \dots |\phi_{s-1}\rangle$ for any $|\phi_i\rangle$ with $i = 1, 2, \dots, s$. For the particular case of $s = 2$ the value of $\text{Tr} \{ \rho^2 \}$ is directly related to the probability of projecting $\rho \otimes \rho$ into its symmetric and antisymmetric subspaces. The values of the 2^n different purities associated with $\rho_{123\dots n}$ can hence be determined from the expectation value of the symmetric and antisymmetric projectors, on each different pair of reduced states $\rho_B = \text{Tr}_A(\rho_{123\dots n})$, where $A \cup B = \{1, 2, \dots, n\}$. These expectation values can be measured without resorting to the implementation of the three-qubit C-Swap gate $C - V^{(2)}$ if two identically prepared 1D rows of n qubits which are represented by bosonic particles are coupled via pairwise BS, as shown in Fig. 2 [9].

The BS in the j -th column projects the symmetric (antisymmetric) part of the density operator ρ_j onto doubly

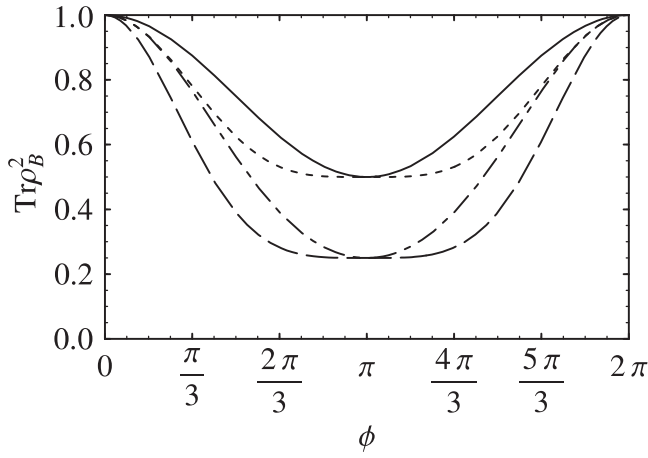


FIG. 1: Effect of varying ϕ on $\text{Tr} \{\rho_B^2\}$ where B is any one atom not at an end (dotted), any two atoms not at ends and with at least two others between them (dashed), any two or more consecutive atoms not including an end (dash-dotted), any one or more consecutive atoms including one end (solid). These purities are independent of n . For $n \geq 6$ corresponding subsets are e.g. $B = \{2\}$, $\{2, 5\}$, $\{2, 3, 4, 5\}$, $\{1, 2, 3, 4, 5\}$, respectively. Hence the state is entangled if the purities as listed above are not in decreasing order that is for all ϕ except integer multiples of 2π .

(singly) occupied sites [18] (for details see Appendix A). Two qubits in column j and in state $\rho_j \otimes \rho_j$ will thus end up in the same site (+) or in different sites (-) with probabilities

$$P_{\pm}^{(j)} = \frac{1}{2} \text{Tr} \{ (\mathbb{I} \pm V^{(2)}) \rho_j \otimes \rho_j \} = \frac{1}{2} \pm \frac{1}{2} \text{Tr} \{ \rho_j^2 \}. \quad (11)$$

Here $S_{\pm} = (\mathbb{I} \pm V^{(2)})/2$ is the symmetric / antisymmetric projector. By distinguishing doubly occupied sites from singly occupied ones we can thus determine the purity of ρ_j .

Extending this two-qubit scenario to the general case of two copies of a state of n qubits undergoing pairwise BS (see Fig. 2) we obtain [9]

$$P_{\pm_1 \pm_2 \dots \pm_n} = \text{Tr} \left\{ \prod_{i=1}^n \frac{\mathbb{I} \pm_i V_i^{(2)}}{2} \rho_{12\dots n} \otimes \rho_{12\dots n} \right\}. \quad (12)$$

Inverting the linear equation Eq. (12) the impurity of any subset of atoms B is given by twice the probability of having an odd number j_B of antisymmetric projections in subset B

$$\text{Tr} \{ \rho_B^2 \} = P(j_B \text{ even}) - P(j_B \text{ odd}) = 1 - 2P(j_B \text{ odd}). \quad (13)$$

For example, for $n = 3$:

$$\text{Tr} \{ \rho_{123}^2 \} = P_{+++} + P_{+--} + P_{-+-} + P_{--+} - P_{---} - P_{++-} - P_{+-+} - P_{-++}, \quad (14)$$

$$\text{Tr} \{ \rho_{12}^2 \} = P_{+++} + P_{++-} + P_{--+} + P_{---} - P_{-++} - P_{-+-} - P_{+-+} - P_{+--}, \quad (15)$$

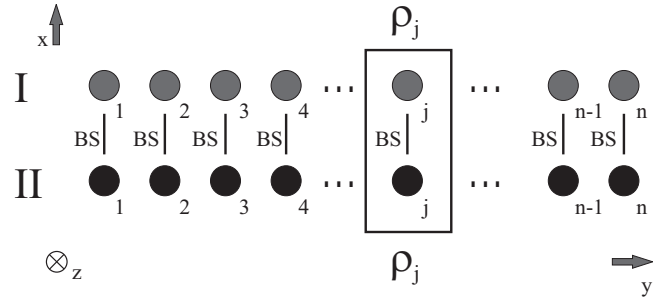


FIG. 2: Entanglement detection network acting on two rows I and II of identical qubits. The two rows of n qubits are prepared in the (possibly entangled) state $\rho_{123\dots n} \otimes \rho_{123\dots n}$ and performing the pairwise BS followed by measuring the lattice site occupancies realizes the entanglement detection network by projecting each operator ρ_j into its symmetric and antisymmetric subspaces.

$$\text{Tr} \{ \rho_1^2 \} = P_{+++} + P_{+--} + P_{-+-} + P_{--+} - P_{---} - P_{++-} - P_{+-+} - P_{-++}. \quad (16)$$

C. Realization in Optical lattices

We consider one sheet in the $x-y$ plane of an ultracold two-species bosonic gas confined in a 3D optical lattice sufficiently deep so that the system is in a Mott insulating state with exactly one atom per lattice site [19]. Two long lived internal states of each atom $|a\rangle$ and $|b\rangle$ represent a qubit, i.e. for a site with row index l and column index j we define two basis states $(a_l^{(j)})^\dagger |\text{vac}\rangle \equiv |0\rangle_l^j$ and $(b_l^{(j)})^\dagger |\text{vac}\rangle \equiv |1\rangle_l^j$. Here $|\text{vac}\rangle$ is the vacuum state and a (b) is the bosonic destruction operator for an atom in internal state $|a\rangle$ ($|b\rangle$). We assume that starting from this Mott state identical multipartite entangled states $\rho_{123\dots n}$ are created in each row while different rows remain uncorrelated. This can e.g. be achieved by state selective cold controlled collisions between atoms in neighboring columns [6, 20]. The above entanglement detection network can be realized in this setup to study the entanglement properties of $\rho_{123\dots n}$. We will first discuss the implementation of the BS by coupling pairs of rows along the x -direction and then investigate methods to distinguish doubly from singly occupied sites. Note that the intrinsic parallelism of the 3D optical lattice will allow to run many copies of these networks in the lattice at once. By exploiting this parallelism one can obtain an estimate of the desired projection probabilities and test the violation of Eqs. (2, 4) in a single or few experimental runs only.

1. The pairwise Beam Splitters

The dynamics of the atoms in the optical lattice is governed by the Bose-Hubbard Hamiltonian (BHM) [19, 20].

We assume that any hopping along the y and z directions is suppressed by a sufficient depth of the lattice in these directions. The hopping in x -direction is controlled by dynamically varying the corresponding lattice depth V_{0x} . Since V_{0x} is proportional to the laser intensity it can easily be changed in the experiment. The pairwise BS requires that rows be coupled pairwise (this can be achieved by using a superlattice of twice the period) and thus we only need to consider one such pair labelling the two rows by I and II , respectively, as shown in Fig. 2.

The Hamiltonian describing the dynamics of the atoms in these two rows can be written as a sum $H_{\text{BHM}} = H_{\text{BS}} + H_U$ where H_{BS} is due to hopping along the x direction and H_U is due to the repulsion between two atoms occupying the same lattice site [19, 20]. The two contributions are given by

$$H_{\text{BS}} = -J \sum_{j=1}^n (a_I^{(j)\dagger} a_{II}^{(j)} + b_I^{(j)\dagger} b_{II}^{(j)} + \text{h.c.}), \quad (17)$$

$$H_U = \sum_{l=I,II} \sum_{j=1}^N \frac{U}{2} a_l^{(j)\dagger} a_l^{(j)\dagger} a_l^{(j)} a_l^{(j)} + \frac{U}{2} b_l^{(j)\dagger} b_l^{(j)\dagger} b_l^{(j)} b_l^{(j)} + U b_l^{(j)\dagger} b_l^{(j)} a_l^{(j)\dagger} a_l^{(j)},$$

where J is the hopping matrix element and U is the onsite interaction energy. The parameters U and J depend on the parameters of the trapping lasers, and their ratio can be varied over a wide range, on time scales much smaller than the decoherence time of the system, by dynamically changing the depth V_0 of the optical lattice [19, 20].

The BS dynamics is perfectly realized in the non-interacting limit $U = 0$ by applying H_{BS} for a time $t_{bs} = \pi/(4J)$ (for details see Appendix A). However, in practice it is impossible either to control J perfectly accurately or to completely turn off the interaction U , and these imperfections cause the symmetric component to have a non-zero probability q_{bs} of failing to bunch which is given by

$$q_{bs} \approx \frac{\pi^2}{8} \left(\frac{\delta J}{J} \right)^2 + \frac{1}{16} \left(\frac{U}{J} \right)^2. \quad (18)$$

Here δJ describe the fluctuations in J (for details see Appendix A). If the fluctuations δJ occur from run to run rather than from site to site q_{bs} can be interpreted as a statistical random variable. We will discuss how to correct this error in Sec. IV.

2. Measuring the lattice site occupation

Recently, a method that uses atom-atom interactions to distinguish between singly and doubly occupied sites was demonstrated experimentally [21]. However, a simplified alternative method where rapid same-site two-atom loss is induced via a Feshbach resonance and the remaining singly-occupied sites are detected suffices for our

purpose. The detection of the remaining singly-occupied sites is achieved by measuring the atomic density profile after the atoms are released from the lattice. A single Feshbach resonance will cause the loss of either $|aa\rangle$, $|ab\rangle + |ba\rangle$, or $|bb\rangle$. Hence, in order to empty doubly-occupied sites in all three states we can either turn on consecutively three separate Feshbach resonances or change the internal state of the pairs of atoms during the loss process using an appropriate sequence of laser pulses. Even if three resonances are experimentally accessible the latter might yield better results as the resonance with the best ratio of two-atom to single-atom loss can be exploited. One suitable sequence [22] which does not require precise control is to apply a large number of pulses of random relative phase and approximate area $\pi/2$ each at equal intervals. Each initial state then spends 1/3 of the time in the resonant state, and hence has probability $q_l = \exp(-t_l/3\tau_d)$ of failing to lose a pair of atoms occupying the same site where t_l is the total duration of the sequence and τ_d the two-atom loss time constant. This method will not be perfect since single particles are also lost from the system with some time constant τ_s and hence t_l cannot be chosen arbitrarily large. The probability of losing a single particle is $p_l = 1 - \exp(-t_l/\tau_s)$ where $\tau_s \gg \tau_d$. Both p_l and q_l are error probabilities, and their sum $p_l + q_l$ is minimized by choosing $t_l = \ln(\tau_s/(3\tau_d))/(1/3\tau_d - 1/\tau_s)$. An experiment recently performed by Widera *et. al* [21] measured $\tau_d = 1.3\text{ms}$ and no detectable loss of single atoms for resonance times up to 100ms. If we take $\tau_s = 500\text{ms}$ the above gives $t_l = 19\text{ms}$ and error probabilities of $q_l = 0.8\%$ and $p_l = 3.7\%$.

In summary, the optical lattice realization of our entanglement detection network contains the following stages at which experimental errors are likely to occur: (i) q_{bs} from the implementation of H_{BS} ; (ii) p_l and q_l occurring during the loss stage; (iii) detector errors p_d in counting the number of singly occupied lattice sites. In addition (iv) the setup might lack spatial resolution in atom counting. We consider how to correct errors (i) - (iii) in Sec. IV and next study the case (iv) of no spatial resolution in an otherwise perfect experimental setup.

III. ENTANGLEMENT DETECTION AND CHARACTERIZATION WITHOUT SPATIAL RESOLUTION

We assume that the measurement of the total number of singly/doubly occupied sites is accurate but that we cannot know their locations. We first show that this information is sufficient to detect a violation of Eq. (4). Then we study how various different experimentally realizable multipartite entangled states might be characterized using such measurements.

A. Entanglement detection

The probabilities $P(j)$ of measuring j singly occupied sites in one row ($2j$ single atoms in total) are given by

$$P(j) = \sum_{|A|=j} \frac{1}{2^n} \sum_B (-1)^{|A \cap B|} \text{Tr} \{ \rho_B^2 \} \quad (19)$$

$$= \frac{1}{2^n} \sum_{k=0}^n \binom{n}{k} \overline{\text{Tr} \{ \rho_{(k)}^2 \}} \sum_l \binom{k}{l} \binom{n-k}{j-l} (-1)^l,$$

where the summation indices are $k = |B|$, $l = |A \cap B|$, $j = |A|$, and A is the set of singly occupied (antisymmetric) sites. We form the generating function

$$\sum_{j=0}^n x^j P(j) = \frac{1}{2^n} \sum_{k=0}^n \binom{n}{k} \overline{\text{Tr} \{ \rho_{(k)}^2 \}} (1-x)^k (1+x)^{n-k}$$

$$= \left(\frac{1+x}{2} \right)^n \sum_{k=0}^n \binom{n}{k} \overline{\text{Tr} \{ \rho_{(k)}^2 \}} \left(\frac{1-x}{1+x} \right)^k \quad (20)$$

and let $y = (1-x)/(1+x)$, to obtain

$$\sum_{j=0}^n (1-y)^j (1+y)^{n-j} P(j) = \sum_{k=0}^n y^k \binom{n}{k} \overline{\text{Tr} \{ \rho_{(k)}^2 \}}, \quad (21)$$

from which we find

$$\overline{\text{Tr} \{ \rho_{(k)}^2 \}} = \left[\binom{n}{k} \right]^{-1} \sum_{j=0}^n P(j) \sum_l \binom{j}{l} \binom{n-j}{k-l} (-1)^l. \quad (22)$$

Therefore, although we cannot determine the purity of a given subset of the row of atoms we can still determine average purities associated with subsets of atoms of a given size by measuring $P(j)$. We will prove later (see Eq. (30)) that the accuracy in finding $P(j)$ required for obtaining a given accuracy of $\overline{\text{Tr} \{ \rho_{(k)}^2 \}}$ has an upper bound independent of n and k if no errors are present. The network is thus efficient in detecting the presence of entanglement in all pure (and some mixed) entangled states via the violation of Eq. (4).

In Fig. 3 we show the probabilities $P(j)$ and the resulting average purities for a variety of different states. For a classically correlated state shown in Fig. 3a the values of $\overline{\text{Tr} \{ \rho_{(k)}^2 \}}$ are monotonically decreasing with k showing that Eq. (4) is not violated. The maximally entangled state shown in Fig. 3b has the characteristic that $\overline{\text{Tr} \{ \rho_{(k)}^2 \}} = 1/2$ for $0 < k < n$ while $\overline{\text{Tr} \{ \rho_{(n)}^2 \}} = 1$ and thus the inequalities are violated in this case. The cluster state shown in Fig. 3c violates the inequalities for all $j > n/2$ and therefore its entanglement is detected. Finally, in Fig. 3d we show a noisy cluster state which was affected by phase noise acting independently on each atom. It can clearly be seen that decoherence reduces the violation of the inequalities but that entanglement is detectable for small amounts of noise.

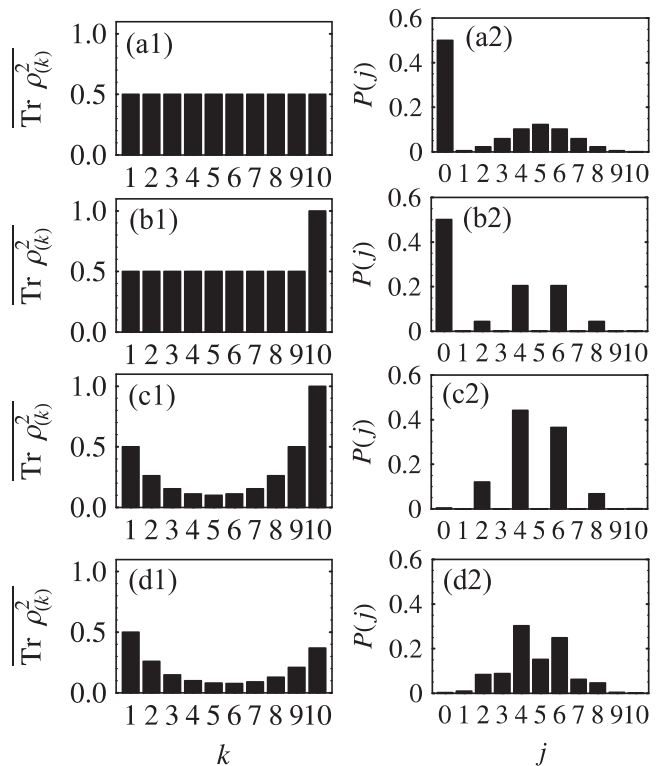


FIG. 3: $\overline{\text{Tr} \{ \rho_{(k)}^2 \}}$ against k (left) and $P(j)$ against j (right) for $n = 10$. (a) Classically correlated state $\rho = (|0\rangle^n \langle 0| + |1\rangle^n \langle 1|)/2$. (b) Maximally entangled state $|\gamma = 0\rangle_{10}$. (c) Cluster state $|\phi = \pi\rangle_{10}$. (d) Same as (c) with 10% dephasing decoherence.

B. Characterization of entanglement

The n measurable quantities $\overline{\text{Tr} \{ \rho_{(k)}^2 \}}$, $k = 1, \dots, n$ do not provide us with enough information to determine an arbitrary state ρ . However, if it may be assumed that the state ρ is of a known form with less than n unknown parameters, it is often possible to determine these parameters from $\overline{\text{Tr} \{ \rho_{(k)}^2 \}}$. We demonstrate this by considering macroscopic superposition states $|\gamma_n\rangle$ and cluster-like states $|\phi_j\rangle$ introduced in Sec. II A 3. Finally, we will also look at product states of states of subsystems containing several atoms.

1. Macroscopic superposition states

Because the state $|\gamma_n\rangle$ is totally symmetric the individual purities given in Eq. (7) only depend on the size of the subsystem $k = |B|$ and thus $\overline{\text{Tr} \{ \rho_{(k)}^2 \}} = \overline{\text{Tr} \{ \rho_B^2 \}}$. Hence, from the knowledge of $\overline{\text{Tr} \{ \rho_{(k)}^2 \}}$ we can determine the value of γ which in principle only requires two of the purities. The remaining equations allow a partial

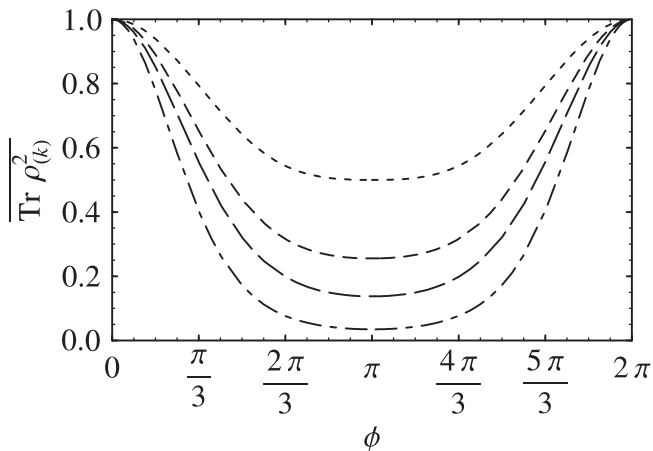


FIG. 4: Average purities $\overline{\text{Tr} \left\{ \rho_{(k)}^2 \right\}}$ ($k = 1$ dotted curve, $k = 2$ dashed curve, $k = 3$ dash-dotted curve, $k = 7$ solid curve) for the state $|\phi_{n=15}\rangle$. Since all states are pure we have $\overline{\text{Tr} \left\{ \rho_{(k)}^2 \right\}} = \overline{\text{Tr} \left\{ \rho_{(n-k)}^2 \right\}}$.

check of the assumption that the measured state indeed has the form $|\gamma_n\rangle$.

2. Cluster states

The states $|\phi_n\rangle$ are parameterized by the entangling phase ϕ . The average purities as a function of ϕ are depicted in Fig. 4. For any value of $0 < \phi < 2\pi$ the states violate the inequalities Eq. (4). The degree of violation increases with ϕ until $\phi = \pi$ where the state is a cluster state and the degree of violation is a maximum. If ϕ is increased further the state again approaches a product state and the degree of violation of the inequalities correspondingly decreases. Hence, from experimentally measured $\overline{\text{Tr} \left\{ \rho_{(k)}^2 \right\}}$ one can determine the phase ϕ up to its sign. Again the over determined system (n equations for one unknown ϕ) provides a check on how well the state fits the assumed form $|\phi_n\rangle$.

The effect of dephasing according to the map Eq. (8) on a cluster state is shown in Fig. 5. The average purities decrease with increasing noise level d . Entanglement is certainly present and in principle detectable by our method as long as the $\overline{\text{Tr} \left\{ \rho_{(k)}^2 \right\}}$ are not in descending order, in the case shown in Fig. 5 up to $d \approx 0.45$. Again, the parameter d can in principle be determined from measuring the average purities.

3. Products of entangled subsystem states

Finally we give an example of a class of states where even though ρ is characterized by more than n param-

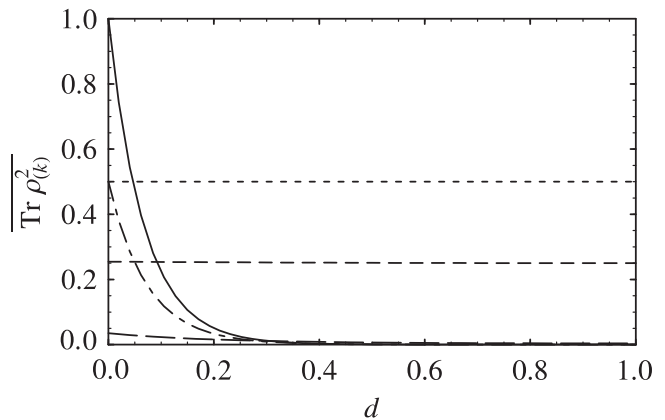


FIG. 5: Effect of dephasing noise on the $n = 15$ cluster state, $k = 1$ (dotted), $k = 2$ (short dashed), $k = 8$ (long dashed), $k = 14$ (dash-dotted), $k = 15$ (solid).

ters, the associated average purities $\overline{\text{Tr} \left\{ \rho_{(k)}^2 \right\}}$ only depend on n parameters. Consider the case where ρ is a product state of L subsystems, $\rho = \otimes_{i=1}^L \rho_i$, with each subsystem ρ_i composed of a known number n_i of atoms. In this case we have

$$\overline{\text{Tr} \left\{ \rho_{(k)}^2 \right\}} = \sum_{\substack{\{k_1, \dots, k_j\} \\ \sum_i k_i = k}} \prod_i \binom{n_i}{k_i} \overline{\text{Tr} \left\{ \rho_{i(k_i)}^2 \right\}}. \quad (23)$$

Since there are $\sum_i n_i = n$ different $\overline{\text{Tr} \left\{ \rho_{i(k_i)}^2 \right\}}$ in total, $\overline{\text{Tr} \left\{ \rho_{(k)}^2 \right\}}$ provides us with enough information to determine the average purities $\overline{\text{Tr} \left\{ \rho_{i(k_i)}^2 \right\}}$ of every subsystem. In particular, $L = n/2$ and all $n_i = 2$ is the case of only pairwise entanglement. Since Eq. (5) holds for all ρ_i taking $n_i = 2$ provides a test for multi-particle as opposed to two-particle correlations in a given state. We note that unless ρ is pure classical multipartite correlations will also be detected by our network.

We will now study how the working of the network is affected by experimental errors. In particular we will estimate how many runs are necessary to obtain the probabilities $P(j)$ with sufficient accuracy in the presence of errors.

IV. EFFECTS OF EXPERIMENTAL ERROR

The errors introduced in Sec. II C affect the ability to find the purities $\overline{\text{Tr} \left\{ \rho_B^2 \right\}}$ as well as the average purities $\overline{\text{Tr} \left\{ \rho_{(k)}^2 \right\}}$ associated with $\rho_{12\dots n}$. All of these errors are of one of two mathematical kinds: extra *pairs* of atoms and missing *single* atoms. We call these two errors “beam-splitter” and “detector” error respectively. Their respective probabilities $q = q_{bs} + q_l$ and $p = p_d + p_l$ are

understood to include also errors occurring while particles are lost from doubly occupied sites. The relationship Eq. (13) between the purities of ρ_B and the probabilities of an even/odd number j_B of singly occupied sites in B indicates that an experimental error, occurring with probability p per site, changes the result $\text{Tr} \{\rho_B^2\}$ by $O(|B|p)$ if we do not attempt to correct for it. This renders the measured results totally meaningless as soon as $|B|p \sim 1$, because the purity of any given state ρ_B is smaller or equal to one. However certain types of error, including the BS and detector errors, can be corrected by a suitable modification of the formulas Eqs. (13, 22) yielding $\text{Tr} \{\rho_B^2\}$ and $\overline{\text{Tr} \{\rho_{(k)}^2\}}$. This correction eliminates systematic errors, making $\text{Tr} \{\rho_B^2\}$ and $\overline{\text{Tr} \{\rho_{(k)}^2\}}$ correct on average, but tends to amplify the random errors that are inevitable in measuring probabilities using a finite number of experimental runs. These random errors can in principle be made arbitrarily small for any $p, q < 1$ by increasing the number of runs, but in practice there is a limit because, as we will show, the number of runs required scales approximately exponentially in $|B|p$. We will now investigate the effects of these errors on the performance of the entanglement detection network both without and with spatial resolution.

A. Without spatial resolution

We assume the probabilities p and q to be the same for all $2n$ lattice sites and in the case of q for all symmetric atom pair states $|aa\rangle$, $|bb\rangle$ and $|ab\rangle + |ba\rangle$. Errors at different lattice sites are assumed to be uncorrelated.

1. Beam splitter error

Let $P_{\text{exp}}(i)$ be the probability of detecting i atoms in an experimental run. If only BS errors are present this probability is given by

$$P_{\text{exp}}(2i) = \sum_{j=0}^i P(j) \binom{n-j}{n-i} q^{i-j} (1-q)^{n-i}, \quad (24)$$

where the factor two in $P_{\text{exp}}(2i)$ accounts for $P(j)$ being the probability of having j antisymmetric pairs. We can use generating functions to invert Eq. (24)

$$\sum_{i=0}^n x^i P_{\text{exp}}(2i) = \sum_{j=0}^n P(j) x^j (1-q+qx)^{n-j}, \quad (25)$$

leading to

$$P(j) = \sum_{i=0}^j \binom{n-i}{n-j} \frac{(-q)^{j-i}}{(1-q)^{n-i}} P_{\text{exp}}(2i). \quad (26)$$

We now apply Eq. (26) to a subsystem B and substitute this into Eq. (13), giving

$$\text{Tr} \{\rho_B^2\} = \sum_{i_B=0}^k \left(\frac{1+q}{1-q} \right)^{k-i_B} (-1)^{i_B} P_{\text{exp}}(2i_B), \quad (27)$$

where i_B refers to the number of atoms detected in B . This expression is then averaged over all B of size $|B| = k$ to give

$$\overline{\text{Tr} \{\rho_{(k)}^2\}} = \sum_{i=0}^n A_{ki} P_{\text{exp}}(2i), \quad (28)$$

with

$$A_{ki} = \left[\binom{n}{k} \right]^{-1} \sum_{l=0}^k (-1)^l \left(\frac{1+q}{1-q} \right)^{k-l} \binom{i}{l} \binom{n-i}{k-l}. \quad (29)$$

Hence, using Eq. (29) instead of Eq. (22) corrects all the *systematic* error caused by an imperfect BS. We are still left with the inherent *random* error associated with the measurement of the probabilities $P_{\text{exp}}(2i)$, which is reduced by increasing the number of experimental runs.

Because of this random error the estimate of $\overline{\text{Tr} \{\rho_{(k)}^2\}}$ obtained from N experimental runs (each using one pair $\rho \otimes \rho$) has the correct mean but a nonzero standard deviation $\sqrt{V_k/N}$, where this defines $V_k(p, q, \rho)$; hence $O(V_k)$ runs are necessary for meaningful results. Note that in general $V_k > 0$ even when $p = q = 0$, as it includes the inherent quantum uncertainty as well as that added by experimental error. In the case of BS error

$$\begin{aligned} V_k &= \sum_i P_{\text{exp}}(i) A_{ki}^2 - \left(\overline{\text{Tr} \{\rho_{(k)}^2\}} \right)^2 < \max_i (A_{ki}^2) \\ &\leq \left(\frac{1+q}{1-q} \right)^{2k} \approx e^{4kq}, \end{aligned} \quad (30)$$

where the approximation is valid for $k \gg 1$, $q \ll 1$. The bound Eq. (30) proves that the number of runs required to obtain meaningful estimates of $\overline{\text{Tr} \{\rho_{(k)}^2\}}$ is reasonable for $k \lesssim 1/q$, however large n is.

We numerically computed the worst case by maximizing V_k with respect to $\overline{\text{Tr} \{\rho_{(k)}^2\}}$ subject only to Eq. (5) and compare it to cluster states $|(\phi = \pi)_n\rangle$ in Fig. 6. The results confirm the analytically found exponential increase of V_k with q in the worst case. For the cluster state V_k increases only slowly with q for small $k \leq 1/q$ while for $k \gtrsim 1/q$ we find approximately exponential growth of V_k with q . We also computed the variances for maximally entangled states and found that they are quite close to the worst case shown in Fig. 7a. Therefore one may in an experiment generally not expect the variances V_k to be much smaller than our worst case results. Thus only BS errors up to $q = 1/k$ are acceptable and yield reliable

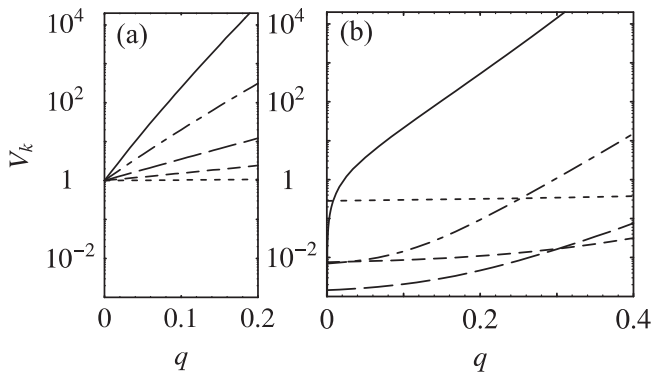


FIG. 6: Variance V_k against BS error, for $k = 1$ (dotted), $k = 4$ (short dashed), $k = 7$ (long dashed), $k = 11$ (dash-dotted), $k = 15$ (solid) curve, and $n = 15$. (a) shows the result for the worst case and (b) for a cluster state.

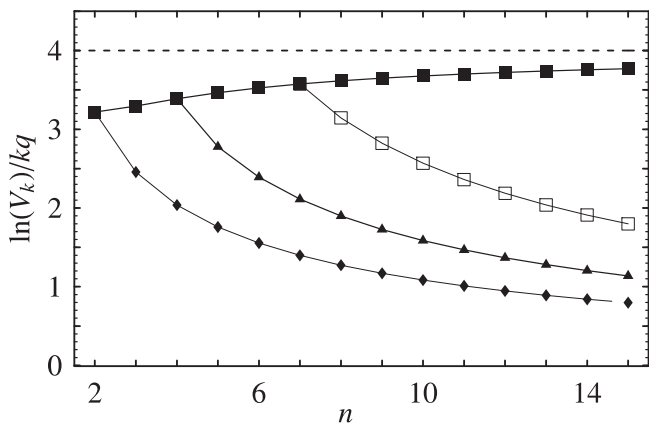


FIG. 7: Worst case variance against n with BS error $q = 1/k$, for $k = 2$ (diamonds), $k = 4$ (triangles), $k = 7$ (hollow squares), $k = n$ (solid squares). The dotted horizontal line is the analytic bound $V_k \leq \exp(4kq)$. The solid curves are drawn to guide the eye.

results in a reasonable number of runs for all $0 \leq k \leq n$. However, as shown in Fig. 7 for $q = 1/k$, the average purities with $k \ll n$ will be determined much more accurately than those with $k \approx n$ and should thus be preferentially used for determining parameters characterizing the measured state.

We finally note that if J is fluctuating from run to run and q_{bs} hence becomes a random variable error correction is still possible. In this case we have to replace Eq. (24) by

$$P_{\text{exp}}(2i) = \sum_{j=0}^i P(j) \binom{n-j}{n-i} \times \int dJ f(J) q(J)^{i-j} (1-q(J))^{n-i}, \quad (31)$$

where $f(J)$ is the probability density function of J and $q(J)$ denotes the BS error as a function of J . The resulting system of linear equations Eq. (31) can be treated

using the methods introduced above.

2. Detector error

We now assume that only detector errors are present and each atom has a probability p of failing to be detected. In this case $P_{\text{exp}}(i)$ is related to $P(j)$ via

$$P_{\text{exp}}(i) = \sum_{j=i/2}^n P(j) \binom{2j}{i} p^{2j-i} (1-p)^i. \quad (32)$$

We can again solve this equation by methods similar to those used in Sec. IV A 1 (though this time it is not a true inverse because the system is over-determined [23]) to obtain

$$P(j) = \sum_{i=2j}^n \binom{i}{2j} \frac{(-p)^{i-2j}}{(1-p)^i} P_{\text{exp}}(i), \quad (33)$$

where non-integer values of j are discarded. By combining Eqs. (22, 33) we obtain $\text{Tr} \left\{ \rho_{(k)}^2 \right\}$ in terms of $P_{\text{exp}}(i)$. For the remaining random error measured by V_k we obtain the upper bound

$$V_k \leq \left(\frac{1+p}{1-p} \right)^{4n} \approx e^{8np}. \quad (34)$$

Numerical calculations for $n \leq 15$ confirm this exponential growth of V_k with p at $np \sim 1$. The results are shown in Fig. 8. This time, however, V_k is typically much smaller than the analytic bound, e.g. for the $n = 15$ cluster state, fitting $V_k \propto \exp(\beta np)$ gives $\beta \approx 2$. However, the exponential growth with n implies a practical limit of $n \sim 1/p$ for any k contrary to the case of BS errors. This scaling can be improved by using the least squares method to handle the over-determined linear system of equations Eq. (32). We do not have an analytic bound analogous to Eq. (34) for the least squares method but numerical calculations for the cluster state and the worst case result in significantly lower values for V_k than those obtained from Eq. (33). Most importantly as shown in Fig. 9 it appears that the scaling of V_k becomes exponential in kp rather than np similarly to the case of BS errors. This implies that an error of $p \lesssim 1/k$ is acceptable for obtaining meaningful estimates of $\text{Tr} \left\{ \rho_{(k)}^2 \right\}$ in a reasonable number of experimental runs.

In an actual experiment both BS and detector errors will be present and first correcting for the detector error p using Eq. (33), then substituting the resulting $P(j)$ for $P_{\text{exp}}(2j)$ in Eq. (29) to correct for the BS error q yields a combined analytical error bound of

$$V_k \leq \left(\frac{1+p}{1-p} \right)^{4n} \left(\frac{1+q}{1-q} \right)^{2k} \approx e^{8np+4kq}. \quad (35)$$

According to our numerical results using the least squares method this bound can be improved requiring only $p, q \lesssim 1/k$ for obtaining sufficiently small errors.

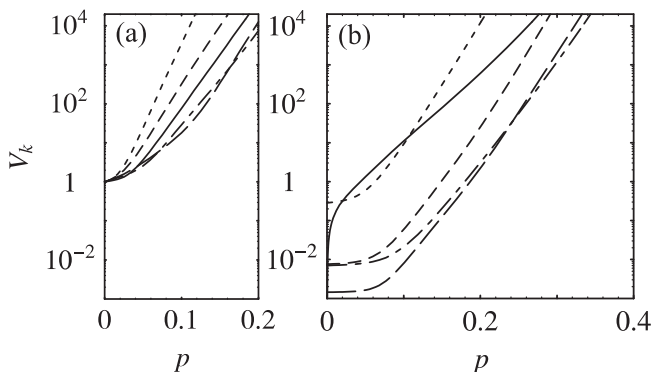


FIG. 8: Variance against detection error without spatial resolution using Eq. (33), for $k = 1$ (dotted), $k = 4$ (short dashed), $k = 7$ (long dashed), $k = 11$ (dash-dotted), $k = 15$ (solid), and $n = 15$. (a) shows the result for the worst case and (b) for a cluster state.

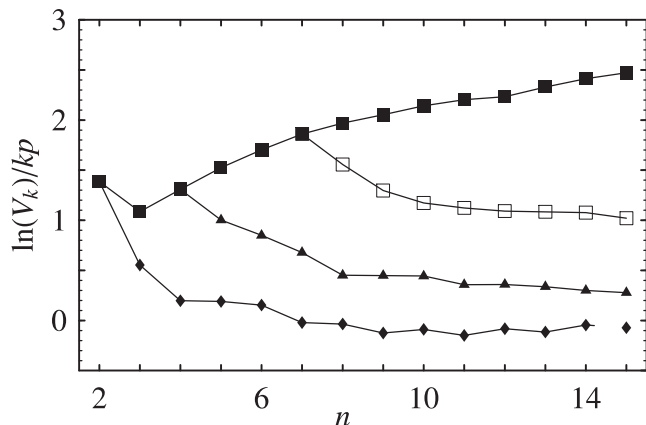


FIG. 9: Worst case variance against n with detection error $p = 1/(2k)$ using least squares, for $k = 1$ (diamonds), $k = 2$ (triangles), $k = 3$ (hollow squares), n (solid squares). The solid curves are drawn to guide the eye.

B. With spatial resolution

If spatial resolution is available then $\text{Tr} \{\rho_B^2\}$, not just its average $\overline{\text{Tr} \{\rho_{(k)}^2\}}$ over all subsets B of size k , becomes accessible to measurement. This allows us to do some state characterizations which would otherwise be impossible and also introduces extra redundancy. As we will show below this does not affect the tolerance to BS errors but we will find that the detector error tolerance improves to $p^2 \sim 1/|B|$. Imperfections in the spatial resolution, however, will lead to additional errors in determining $\text{Tr} \{\rho_B^2\}$.

1. Beam splitter error

The variance of $\text{Tr} \{\rho_B^2\}$ due to BS errors can be directly inferred from Eq. (27), where only the atoms in B

are counted. Using the same methods as in Sec. IV A 1 we find an upper bound for V_B (defined analogously to V_k) given by $V_B \leq ((1+q)/(1-q))^{2|B|} \approx \exp(4|B|q)$. The BS error tolerance (for fixed $k = |B|$) is thus independent of whether spatial resolution is available or not.

2. Detector error

The situation is different for the detector error. Each antisymmetric pair contains two atoms only one of which needs to be detected to know that it was antisymmetric. Therefore the effective error probability becomes p^2 . The resulting formula is

$$\text{Tr} \{\rho_B^2\} = \sum_{i=0}^{|B|} (-1)^i \left(\frac{1+p^2}{1-p^2} \right)^i P_{\text{exp}}^B(i), \quad (36)$$

where $P_{\text{exp}}^B(i)$ is the probability of measuring i antisymmetric sites in subset B . The variance bound is given by $V_B \leq ((1+p^2)/(1-p^2))^{2|B|} \approx \exp(4|B|p^2)$.

3. Imperfect spatial resolution

There is a new type of error to consider as the spatial resolution itself will not in practice be perfect. If we let $f(x, y)$ be the probability of finding at position x a particle which is actually at position y , then

$$P_{\text{exp}}(A) = \sum_{i \in B} \sum_{\zeta} \frac{1}{s(A)} \prod_{i=0}^k f(A_{\zeta(i+k)}, B_i) f(A_{\zeta(i)}, B_i) P(B), \quad (37)$$

where A is the “set” (its elements are not necessarily distinct) of observed atom positions, and $P_{\text{exp}}(A)$ is the experimental probability of observing atoms exactly at these positions A . The set B denotes the antisymmetric sites and the probability of having antisymmetric sites at positions B is $P(B)$, $k = |B| = |A|/2$, and ζ runs over all $(2k)!$ permutations of the $2k$ atoms in A . The i -th element of B and A are written as B_i and A_i , respectively. The symmetry factor $s(A)$ stands for the number of permutations ζ which leave the ordered lists of atoms $\{A_i\}$ invariant (e.g., $s(\{1, 1\}) = 2$, $s(\{1, 2\}) = 1$), and is needed because our summation runs over different ordered lists $\{A_i\}$ of the same set A . This is an over-determined linear system, and just as in the case of detector error, we can either explicitly solve it by discarding some of the equations or apply the least squares method. As an explicit solution we can e.g. use

$$P(B) = \sum_{\{A_i\}} \frac{s(A)}{2^k} \left(\prod_{i=1}^{2k} f^{-1}(B_i, A_i) \right) P_{\text{exp}}(A), \quad (38)$$

where we define $B_{k+i} \equiv B_i$. The sum runs over all ordered lists $\{A_i\}$ and f^{-1} is the matrix inverse of f , that is $f^{-1}(y, x)f(x, z) = \delta_{xz}$.

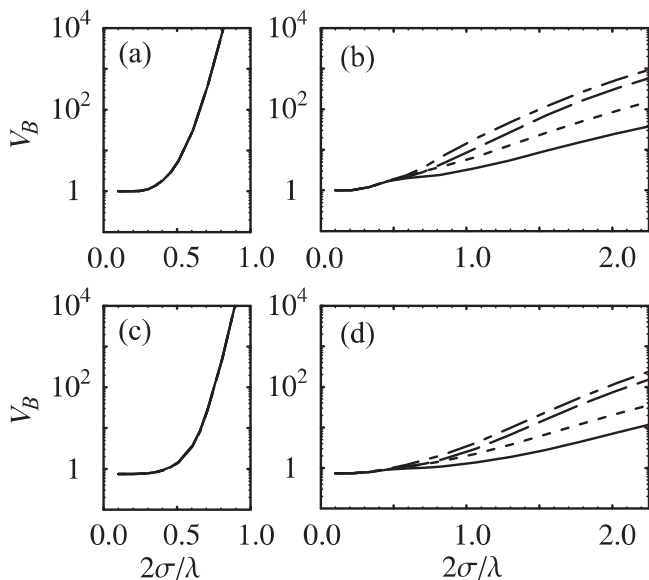


FIG. 10: Variance of $\text{Tr} \{\rho_B^2\}$ as a function of the standard deviation σ , for $B = \{2\}$ (dotted), $B = \{2, 3\}$ (dashed), $B = \{1, 3\}$ (dash-dotted), $B = \{1, 2, 3\}$ (solid), and $n = 4$. (a) and (b) are worst case variances while (c) and (d) are for a maximally entangled state. (a) and (c) each show four almost coincident curves obtained from Eq. (38) while (b) and (d) are found by the least squares method.

As before by performing numerical calculations using the least squares method we find much lower variances than with Eq. (38). An example is shown in Fig. 10 where we plot the variance of $\text{Tr} \{\rho_B^2\}$ due to a Gaussian position error of the form

$$f(x, y) = \frac{1}{\sqrt{2\pi}\sigma} \int_{x-\lambda/4}^{x+\lambda/4} dz \exp[-(z-y)^2/(2\sigma^2)] \quad (39)$$

where σ is the standard deviation and λ is the wave length of the laser creating the optical lattice. The corresponding lattice spacing is $\lambda/2$. The results obtained from Eq. (38) shown in Fig. 10a, c require a resolution of $\sigma \lesssim \lambda/2$ whereas the least squares method shown in Fig. 10b, d yields reasonable variances V_B for spatial resolutions up to $\sigma \lesssim 3\lambda/2$. However, due to the exponentially large number of possibilities for A the least squares calculation becomes intractable for large n .

V. CONCLUSION

We discussed the detection and characterization of multipartite entanglement in optical lattices with the quantum network introduced in [9] under different experimental conditions. We first described how the network can be implemented in ideal experimental conditions and showed that it allows to characterize a number of important classes of states like cluster-like states and

macroscopic superposition states. We investigated the experimental realization of the network in an optical lattice and identified lack of spatial resolution, errors in the BS operation and imperfect atom detection as the main sources of error. We showed that even in the absence of spatial resolution entanglement can be detected. In cases where the entangled state is characterized by a few parameters only we found that these can often be determined from the measurement results. We also studied the influence of BS errors occurring with probability q and detection errors with probability p and concluded that with small numbers of experimental runs entanglement can be detected between k atoms as long as $kp \lesssim 1$ and $kq \lesssim 1$. Finally we showed that for obtaining purities $\text{Tr} \{\rho_B^2\}$ of subsets B rather than average purities with reasonable experimental effort a spatial resolution of $\sigma \approx \lambda$ is necessary.

The results obtained in this work show that unambiguous multipartite entanglement detection in optical lattices is possible with current technology. This has not yet been achieved experimentally [6]. Furthermore it will even be possible to determine some of the characteristics of entangled states created in these experiments without the requirement of performing spatially resolved measurements. Our network is thus a viable alternative to detecting entanglement via witnesses or full quantum state tomography.

Acknowledgments

This work was supported by EPSRC through the QIP IRC (www.qipirc.org) GR/S82176/01 and project EP/C51933/1, and by the EU network OLAQUI. C.M.A. thanks Artur Ekert for useful discussions and is supported by the Fundação para a Ciência e Tecnologia (Portugal).

APPENDIX A: THE BEAM SPLITTER OPERATION

Since the BS only couples two lattice sites in rows I and II of each column (see Fig. 2) we consider a single such pair and omit the column superscript j in this section. For $U = 0$, we obtain from the Heisenberg equations for the operators $\alpha = a, b$

$$\begin{aligned} \alpha_I(t) &= \cos(Jt)\alpha_I - i \sin(Jt)\alpha_{II}, \\ \alpha_{II}(t) &= \cos(Jt)\alpha_{II} - i \sin(Jt)\alpha_I. \end{aligned} \quad (\text{A1})$$

Hence, applying H_{BS} for a time $t_{bs} = \pi/(4J)$ implements a perfect pairwise BS.

Initially the atom pair is in a state of the form $\rho \otimes \rho$, where ρ is a single qubit state and hence has a spectral decomposition of the form $\rho = \lambda_1 |c\rangle \langle c| + \lambda_2 |d\rangle \langle d|$, with $\lambda_1 + \lambda_2 = 1$, $|c\rangle = c^\dagger |\text{vac}\rangle$, and $|d\rangle = d^\dagger |\text{vac}\rangle$. Here c^\dagger, d^\dagger are linear superpositions of a^\dagger, b^\dagger with coefficients

depending on ρ . Therefore we can write

$$\begin{aligned} \rho \otimes \rho &= \lambda_1^2 |c_I c_{II}\rangle \langle c_I c_{II}| + \lambda_2^2 |d_I d_{II}\rangle \langle d_I d_{II}| \quad (\text{A2}) \\ &+ \frac{\lambda_1 \lambda_2}{2} (|c_I d_{II}\rangle + |d_I c_{II}\rangle) (\langle c_I d_{II}| + \langle d_I c_{II}|) \\ &+ \frac{\lambda_1 \lambda_2}{2} (|c_I d_{II}\rangle - |d_I c_{II}\rangle) (\langle c_I d_{II}| - \langle d_I c_{II}|), \end{aligned}$$

which is a classical mixture of a symmetric state with probability $P_+ = 1 - \lambda_1 \lambda_2$ and an antisymmetric state with probability $P_- = \lambda_1 \lambda_2$. After the BS the resulting state $\rho' = \exp(iH_{BS}t)\rho \otimes \rho \exp(-iH_{BS}t)$ is given by

$$\begin{aligned} \rho' &= \lambda_1^2 |\Phi_1\rangle \langle \Phi_1| + \lambda_2^2 |\Phi_2\rangle \langle \Phi_2| \quad (\text{A3}) \\ &+ \lambda_1 \lambda_2 |\Phi_3\rangle \langle \Phi_3| + \lambda_1 \lambda_2 |\Phi_4\rangle \langle \Phi_4|, \end{aligned}$$

where $|\Phi_1\rangle = (c_I^\dagger c_I^\dagger + c_{II}^\dagger c_{II}^\dagger) |\text{vac}\rangle / 2$, $|\Phi_2\rangle = (d_I^\dagger d_I^\dagger + d_{II}^\dagger d_{II}^\dagger) |\text{vac}\rangle / 2$, $|\Phi_3\rangle = (c_I^\dagger d_{II}^\dagger + c_{II}^\dagger d_I^\dagger) |\text{vac}\rangle / \sqrt{2}$ are states with double occupancy in one row and an empty site in the other row while $|\Phi_4\rangle = (c_I^\dagger d_{II}^\dagger - c_{II}^\dagger d_I^\dagger) |\text{vac}\rangle / \sqrt{2}$ is a state with a singly occupied site

in each row. Hence, after the BS we will find a doubly occupied site with probability $1 - \lambda_1 \lambda_2 = P_+$ while two singly occupied sites result with probability $\lambda_1 \lambda_2 = P_-$.

However, in practice it is impossible to completely turn off the interaction U which may result in a symmetric state failing to bunch. We consider any symmetric state $|\Psi_s\rangle$ and because $H_{BS} + H_U$ acts only on the row indices, not the internal states, and is symmetric between the two rows the probability q_{bs} of failure to bunch is given by

$$\begin{aligned} q_{bs} &= |\langle \Psi_s | e^{i(H_{BS} + H_U)t} | \Psi_s \rangle|^2 \quad (\text{A4}) \\ &= \frac{16J^2}{16J^2 + U^2} \cos^2(\sqrt{16J^2 + U^2} \frac{t_{bs}}{2}) \\ &\quad + \frac{U^2}{16J^2 + U^2}. \end{aligned}$$

The optimal choice for the BS time is $t_{bs} = \pi / \sqrt{16J^2 + U^2}$ for which $q_{bs} = U^2 / (16J^2 + U^2)$. If the hopping term is not controlled perfectly accurately but fluctuates by δJ around a mean J we set $t_{bs} = \pi / \sqrt{16J^2 + U^2}$ and obtain Eq. (18).

-
- [1] D. Gottesman, Ph.D thesis (CalTech, Pasadena, 1997); A.M. Steane Phys. Rev. Lett. **77**, 793 (1996); A.R. Calderbank, P.W. Shor, Phys. Rev. A **54**, 1098 (1996).
- [2] R. Cleve, D. Gottesman, H.-K. Lo, Phys. Rev. Lett. **83**, 648 (1999); D. Gottesman, Phys. Rev. A **61**, 042311 (2000); A. Cabello, Phys. Rev. Lett. **89** 100402 (2002).
- [3] R. Raussendorf, H.-J Briegel, Phys. Rev. Lett. **86**, 910 (2001); R. Raussendorf, H.-J Briegel, Phys. Rev. Lett. **86**, 5188 (2001).
- [4] P. Walther, K. J. Resch, T. Rudolph, E. Schenck, H. Weinfurter, V. Vedral, M. Aspelmeyer, A. Zeilinger, Nature **434**, 169 (2005).
- [5] C. A. Sackett *et al.*, Nature **404**, 256 (2000); J. Chiaverini *et al.*, Nature **432**, 602 (2004).
- [6] O. Mandel *et al.*, Nature **425**, 937 (2003); D. Jaksch, H.-J. Briegel, J.I. Cirac, C.W. Gardiner, P. Zoller, Phys. Rev. Lett. **82**, 1975 (1999).
- [7] S.E. Sklarz, I. Friedler, D.J. Tannor, Y.B. Band, C.J. Williams, Phys. Rev. A **66**, 053620 (2002); S. Peil *et al.*, Phys. Rev. A **67**, 051603(R) (2003); W.K. Hensinger *et al.*, Nature **412**, 52 (2001).
- [8] Daniel F. V. James, Paul G. Kwiat, William J. Munro, Andrew G. White, Phys. Rev. A, **64**, 052312 (2001).
- [9] C. Moura Alves and D. Jaksch, Phys. Rev. Lett. **93**, 110501 (2004).
- [10] J. S. Bell, Physics **1** 195, 1964; A. Aspect, P. Grangier, G. Roger, Phys. Rev. Lett. **49**, 91 (1982).
- [11] B. Terhal, Phys. Lett. A **271**, 319 (2000); M. Lewenstein, B. Kraus, J.I. Cirac, P. Horodecki, Phys. Rev. A **62**, 052310 (2000).
- [12] M. Horodecki, P. Horodecki, R. Horodecki, Physics Letters A, **210**, 377 (1996).
- [13] J. I. Cirac, M. Lewenstein, K. Molmer, and P. Zoller, Phys. Rev. A **57**, 1208 (1998).
- [14] C. H. van der Wal *et al.*, Science **290**, 773 (2000); J. R. Friedman, V. Patel, W. Chen, S. K. Tolpygo, and J. E. Lukens, Nature **406**, 43 (2000).
- [15] W. Dür, C. Simon, J.I. Cirac, Phys. Rev. Lett., **89**, 210402 (2002).
- [16] R.F. Werner, Phys. Rev. A **40**, 4277 (1989).
- [17] A.K. Ekert *et al.*, Phys. Rev. Lett. **88**, 217901 (2002); C. Moura Alves, D.K.L. Oi, P. Horodecki, A.K. Ekert, L.C. Kwek, Phys. Rev. A **68**, 032306 (2003).
- [18] In the case of photon pairs this effect is known as Hong-Ou-Mandel interference and used in Bell state analysers: C. K. Hong, Z. Y. Ou, L. Mandel, Phys. Rev. Lett. **59**, 2044 (1987); Klaus Mattle, Harald Weinfurter, Paul G. Kwiat, Anton Zeilinger, Phys. Rev. Lett. **76**, 4656 (1996).
- [19] D. Jaksch, C. Bruder, J.I. Cirac, C.W. Gardiner, P. Zoller, Phys. Rev. Lett. **81**, 3108 (1998); M. Greiner, O. Mandel, T. Esslinger, T.W. Haensch, I. Bloch, Nature **415**, 39 (2002).
- [20] For a review of optical lattices, see D. Jaksch and P. Zoller, Annals of Physics **315**, 52 (2005); D. Jaksch, Contemporary Physics **45**, 367 (2004); I. Bloch, Physics World, **17**, 25 (2004).
- [21] A. Widera *et al.*, cond-mat/0310719.
- [22] If the resonant state is either $|aa\rangle$ or $|bb\rangle$ then there is also a suitable sequence of few pulses, which does not require phase locking, interleaved with suitable loss intervals: (i) a π pulse that swaps $|aa\rangle$ and $|bb\rangle$ (ii) a $\pi/2$ pulse that takes $|ab\rangle + |ba\rangle$ to $|aa\rangle - |bb\rangle$, followed by (iii) a second π pulse.
- [23] In a perfect experiment an even number $2j$ of atoms (two per antisymmetric pair) is always detected but in the presence of detector error an odd number of atoms might arise.